Research Square

Preprints are preliminary reports that have not undergone peer review.
They should not be considered conclusive, used to inform clinical practice,
or referenced by the media as validated information.

Research on the Behavior and Modified Formula of the Longitudinal Deformation Curve in Surrounding Rock of Three-Dimensional Inclined Roadways

Xin Ge
Chongqing Jiaotong University
LINFENG F. WANG
wanglinfeng715@163.com

Chongqing Jiaotong University
Xiaorui Li
University of Emergency Management
Kaiqi Yang
Chongqing Jiaotong University
Mingfei Wu
Chongqing Jiaotong University
Dan Liu
Chongqing Jiaotong University

Research Article

Keywords: Inclined shaft, Three-dimensional stress, Longitudinal deformation profile (LDP), Spatial effect of excavation face, Displacement release coefficient

Posted Date: March 11th, 2026

DOI: https://doi.org/10.21203/rs.3.rs-8967982/v1

License: This work is licensed under a Creative Commons Attribution 4.0 International License. Read Full License

Additional Declarations: No competing interests reported.

Research on the Behavior and Modified Formula of the Longitudinal Deformation Curve in Surrounding Rock of Three-Dimensional Inclined Roadways

Abstract: To provide theoretical support for determining the installation timing and stability analysis of support structures for surrounding rock in inclined mine circular roadways, this study takes the inclined mine circular roadway as the research object. The research reveals the influence laws of the coupling between geological structural factors and mechanical parameters on the Longitudinal Deformation Profile (LDP) curve of the inclined mine circular roadway in three-dimensional space. A modified formula for the LDP curve of the inclined mine circular roadway, incorporating the coupling of geological structural factors and mechanical parameters in three-dimensional space, is proposed. The results indicate that the geological structural factors α and β, along with the shear strength parameters of the rock mass, have a significant impact on the shape of the LDP curve. The influence range of parameter α on the LDP curve morphology is between X/R = -6 and 6. The influence range of parameters β, cohesion, and internal friction angle on the LDP curve morphology is between X/R = -6 and 9. The axial lateral pressure coefficient, horizontal lateral pressure coefficient, and elastic modulus have a relatively minor influence on the shape of the LDP curve. The influence of Poisson's ratio on the displacement release factor is mainly concentrated near the excavation face, affecting the LDP curve morphology within the range of X/R = -1 to 3. A comparison between the proposed modified fitting formula and numerical simulation results shows that this fitting formula can effectively predict the spatiotemporal distribution of surrounding rock deformation.

Keywords: Inclined shaft; Three-dimensional stress; Longitudinal deformation profile (LDP); Spatial effect of excavation face; Displacement release coefficient

1 Introduction

With the extraction of coal resources extending into deeper regions, the scale and burial depth of mine roadways have increased dramatically, leading to increasingly complex three-dimensional stress environments in the surrounding rock. Deep mines therefore commonly face severe challenges such as large deformations of the surrounding rock and failure of support structures, which impose higher demands on roadway stability analysis and support design. In this context, the convergence-confinement method, which is suitable for deep-buried roadways, remains a convenient and practical design approach due to its clear theoretical basis and its ability to reflect the interaction between the surrounding rock and the support[1]. As the core of this method, the longitudinal deformation profile (LDP) can characterize the spatial effects of the tunnel excavation face, serving as a key theoretical foundation for analyzing support timing and evaluating the self-bearing capacity of the surrounding rock.

Currently, the LDP curve has been extensively studied by scholars both domestically and internationally. Song F[2] provided a general numerical method for predicting the longitudinal deformation profile using a coupled viscoelastic-viscoplastic strain-softening model to simulate the progressive damage process and creep failure behavior of rock masses. Wang Jiachen[3] derived

an empirical formula for the displacement release coefficient based on the response surface method, verifying the feasibility of their approach through comparisons with field monitoring and other theoretical results. Ren Zijian[4] used a point load tester to determine the uniaxial compressive strength of argillaceous siltstone in a specific tunnel section, and conducted stability analysis of the initial support by combining the surrounding rock longitudinal deformation curve, the ground reaction curve, and the support characteristic curve. Yu Yongjie[5] analyzed tunnel surrounding rock stability based on the convergence-confinement principle, focusing on two factors: the presence or absence of support installation and the timing of its installation. Wang J[6] investigated the spatial effect of the tunnel excavation face based on the LDP curve, establishing and verifying a calculation method for the lost displacement. Li G[7] studied the deformation characteristics of a typical deep roadway in the inclined rock strata of the Jinchuan Mine through field investigation, theoretical analysis, similar model tests, and numerical simulation. Chen L[8] measured the uniaxial and triaxial compressive strengths of field-sampled rocks through laboratory tests, and combined the results of field acoustic tests and laboratory experiments to study the longitudinal deformation profile of a large-cross-section tunnel under high in-situ stress. Sun Wang[9] used FLAC^{3D} to study the influence of factors such as rock mass parameters and stress conditions on the longitudinal deformation of an unsupported circular tunnel. Liang Yiwen[10] considered Poisson's ratio, elastic modulus, cohesion, internal friction angle, and blasting parameters in their research on the equation for the surrounding rock longitudinal deformation curve, and used FLAC^{3D} to analyze and improve the rationality and effectiveness of the modified equation. Xue Long[11] proposed a numerical testing method that allows arbitrary control of the magnitude and direction of principal stresses in three-dimensional space. He conducted numerical tests on three-dimensional rotation of principal stresses and, based on in-depth analysis, established a constitutive model that considers the effect of three-dimensional principal stress rotation. Qian J[12], Zhe Mei[13], Liu Chao[14], and Jamil F[15] conducted tests on different specimens and found that the direction of the principal stress axis affects the strength and deformation of the specimens. Li Liang[16] conducted systematic research on surrounding rock control technology under weak mining conditions involving principal stress deflection. Liu Jiashun[17] established a numerical calculation model for the excavation disturbance of weakly cemented soft rock roadways, studied the evolution law of the magnitude and direction of principal stresses in the surrounding rock induced by roadway excavation, and determined the loading state parameters for the excavation disturbance rotational stress path tests.

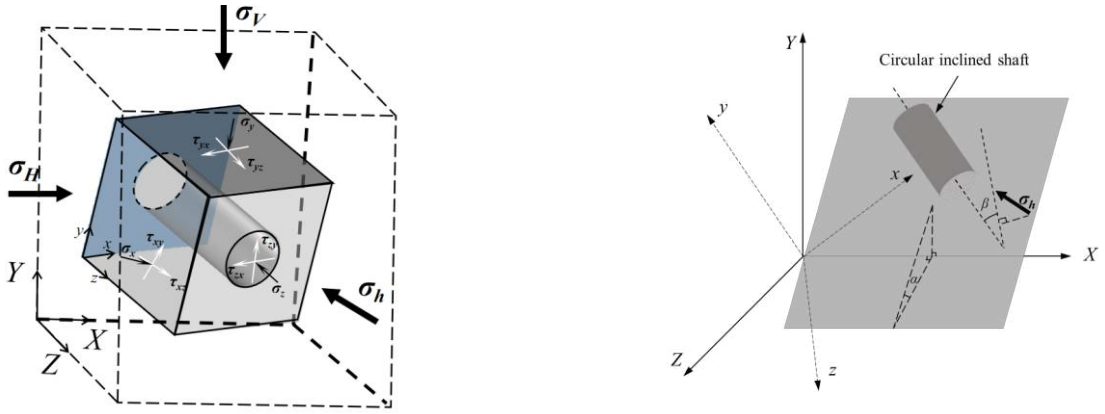
Most of the aforementioned studies on the LDP curve are based on horizontal tunnels as the engineering context, with little consideration given to the spatial effects of the excavation face during the tunneling process of inclined shafts in three-dimensional space. During the excavation of an inclined shaft, the direction of excavation has a certain angle with the horizontal plane, which increases the complexity of studying the longitudinal deformation patterns of inclined shafts. To address these issues, this paper takes the circular inclined shaft as the research object. Considering various rock mass parameters in three-dimensional space, theoretical analysis and numerical simulation methods are employed to construct a three-dimensional

excavation model of a circular inclined shaft. The study aims to reveal the patterns of the LDP curve for circular inclined shafts in three-dimensional space and proposes a modified formula for the LDP curve under the combined influence of spatial and rock property parameters. The findings can provide certain references for the study of construction support in similar engineering projects.

2 Three-Dimensional LDP curve model for circular tunnels in inclined shafts

2.1 Mechanical model for circular tunnels in inclined shafts

The deformation of surrounding rock after roadway excavation is primarily attributed to stress redistribution caused by the excavation. Therefore, it is essential to fully understand the principal stress distribution patterns in the surrounding rock of the tunnel to mitigate such damage[18]. For inclined circular tunnels, stress concentrations form at the periphery of the surrounding rock. The excavation direction is inclined at a certain angle to the horizontal plane, and adjustments involving both the maximum and minimum horizontal in-situ stresses are involved. This makes the stress distribution model in the surrounding rock complex, and its theoretical analysis has long been a challenging problem. To facilitate the analytical process, based on previous studies[18-22], certain conditions are simplified, and the following mechanical assumptions are made: (1) There are no additional roadways in the vicinity of the research subject. (2) The surrounding rock is homogeneous. (3) The cross-sectional shape of the roadway is circular.



(a) Three-dimensional mechanical model of the circular inclined shaft (b) Schematic diagram of the model's spatial position

Fig. 1. Three-dimensional mechanical model and spatial position schematic diagram of the circular inclined shaft.

Because the direction of principal stresses changes near the circular inclined shaft, direct analysis would complicate the stress distribution model in the surrounding rock. To simplify the stress state of the surrounding rock, based on the coordinate transformation theory of elasticity, the coordinate system is aligned with the z-axis parallel to the shaft axis. Considering the spatial position of the circular inclined shaft within the three-dimensional stress field, a three-dimensional mechanical model of the circular inclined shaft is established. The three-dimensional mechanical model and spatial position schematic of the circular

inclined shaft are shown in Fig. 1.

In Fig.1(a), σ_V represents the vertical in-situ stress, σ_H denotes the maximum horizontal in-situ stress, and σ_h indicates the minimum horizontal in-situ stress; σ_x, σ_y, and σ_z represent the normal stresses on each plane parallel or perpendicular to the shaft axis; τ_{xy}, τ_{yz}, and τ_{zx} denote the shear stresses within the planes. In Fig.1(b), α represents the angle between the plane of the circular inclined shaft and the horizontal plane; β denotes the angle between the shaft axis and the projection of σ_h onto the plane of the circular inclined shaft. The spatial parameters α and β can be used to determine the exact position of the circular inclined shaft within the stress space.

According to the geometric relationships and mechanical analysis associated with triaxial stress conditions[23], the stress expression for the mechanical model of the circular inclined shaft is as follows:

$$\begin{cases} \sigma_x = \sigma_H \cos^2\beta + \sigma_h \cos^2\alpha \sin^2\beta + \sigma_v \sin^2\alpha \sin^2\beta \\ \sigma_y = \sigma_h \sin^2\alpha + \sigma_v \cos^2\alpha \\ \sigma_z = \sigma_H \sin^2\beta + \sigma_h \cos^2\alpha \cos^2\beta + \sigma_v \sin^2\alpha \cos^2\beta \\ \tau_{yz} = \sqrt{\sigma_h{}^2 \sin^2\alpha + \sigma_v{}^2 \cos^2\alpha - \sigma_y{}^2}\cos\beta \\ \tau_{yx} = \sqrt{\sigma_h{}^2 \sin^2\alpha + \sigma_v{}^2 \cos^2\alpha - \sigma_y{}^2}\sin\beta \\ \tau_{zx} = \sqrt{(\sigma_H{}^2 + \sigma_h{}^2 \cos 2\alpha - \sigma_v{}^2 \cos 2\alpha - \sigma_x{}^2 + \sigma_y{}^2 - \sigma_z{}^2)/2} \end{cases} \quad (1)$$

As shown in Equation (1), as the angles between the plane of the inclined circular tunnel and the horizontal and vertical planes change, the triaxial stresses in the surrounding rock undergo adjustments, leading to variations in the local stress environment from a mechanical perspective. Considering the differences in triaxial stresses, the stress state and deformation characteristics of the surrounding rock may vary significantly at different distances from the tunnel center. This implies that even under identical in-situ stress conditions, altering the spatial orientation of the tunnel can induce different stress states in the far-field. When analyzing the mechanical behavior of the surrounding rock near the tunnel, it is essential to account for the spatial layout of the tunnel, as the stress state of the surrounding rock transitions from the triaxial in-situ state in the far-field to a distinct state in the near-field closer to the tunnel periphery.

To further the investigation, a finite-length circular inclined shaft is taken as the object of study. Based on the superposition principle of elastic field variables, its stress field is simplified into the superposition of three simpler stress fields. The complex three-dimensional stress field of the circular inclined shaft is thus simplified into the superposition of three fundamental stress fields: the plane strain mechanical model of the circular inclined shaft, the shear mechanical model of the circular inclined shaft, and the uniaxial compression mechanical model. In the figure, σ_{z1} and σ_{z2} represent the components of σ_z along the axial direction of the circular inclined shaft. Figure 2 illustrates the simplified stress field of the circular inclined shaft.

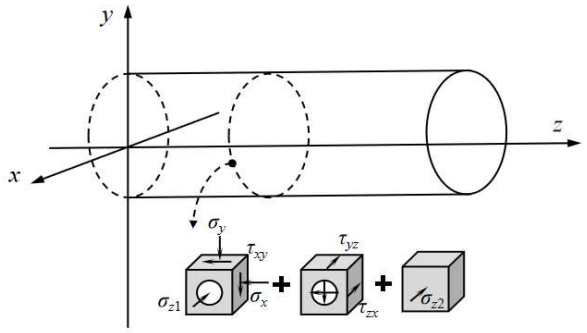


Fig. 2 Simplified diagram of the stress field in the circular inclined shaft.

Fig.3 illustrates the plane strain mechanical model of the circular inclined shaft, where σ_r, σ_θ, and $\tau_{r\theta}$represent the radial stress, tangential stress, and shear stress of the micro-element in polar coordinates, respectively; R denotes the radius of the circular inclined shaft; the radial vector r indicates the distance between the micro-element and the center of the shaft; and θ represents the angle between the radial vector r and the horizontal direction.

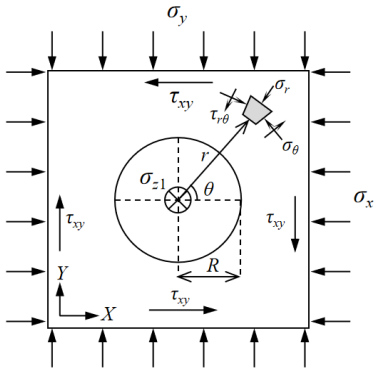


Fig. 3. Plane strain mechanical model of the circular inclined shaft.

Fig.3 shows the plane strain mechanical model of the circular inclined shaft. The plane strain problem described can be simplified into a planar model[24], and mechanical analysis is conducted using micro-elements. The stress expression is derived through the generalized plane strain theory [25]， in the equation, *v* represents Poisson's ratio.

$$\begin{aligned}
\sigma_r &= \frac{\sigma_x+\sigma_y}{2}(1-\frac{R^2}{r^2})+\frac{\sigma_x-\sigma_y}{2}(1+3\frac{R^4}{r^4}-4\frac{R^2}{r^2})\cos(2\theta)+\tau_{xy}(1+3\frac{R^4}{r^4}-4\frac{R^2}{r^2})\sin(2\theta)\\
\sigma_\theta &= \frac{\sigma_x+\sigma_y}{2}(1+\frac{R^2}{r^2})+\frac{\sigma_y-\sigma_x}{2}(1+3\frac{R^4}{r^4})\cos(2\theta)+\tau_{xy}(1+3\frac{R^4}{r^4})\sin(2\theta)\\
\tau_{r\theta} &= -\frac{\sigma_x-\sigma_y}{2}(1-3\frac{R^4}{r^4}+2\frac{R^2}{r^2})\sin(2\theta)+\tau_{xy}(1-3\frac{R^4}{r^4}+2\frac{R^2}{r^2})\cos(2\theta)\\
\sigma_{z1} &= \nu[\sigma_x+\sigma_y-2(\sigma_x-\sigma_y)\frac{R^2}{r^2}\cos(2\theta)+4\tau_{xy}\frac{R^2}{r^2}\sin(2\theta)]
\end{aligned} \tag{2}$$

To obtain the stress solution for the shear mechanical model of the circular inclined shaft, the equilibrium equation (3) is established.

$$\begin{cases} \tau_{rz} = \left(\tau_{zx}\cos\theta + \tau_{yz}\sin\theta\right)\left(1-\dfrac{R^2}{r^2}\right) \\ \tau_{\theta z} = \left(-\tau_{zx}\sin\theta + \tau_{yz}\cos\theta\right)\left(1+\dfrac{R^2}{r^2}\right) \end{cases} \quad (3)$$

The stress expression for the uniaxial compression mechanical model can be derived from the following formulas:

$$\sigma_{z2} = E\varepsilon \quad (4)$$

Here, E represents the elastic modulus of the rock mass, and ε denotes the axial strain under the action of σ_{z2}. According to Hooke's law under plane strain conditions[26]:

$$\dot{o}_r = \frac{1-\nu^2}{E}\left(\sigma_r - \frac{\nu}{1-\nu}\sigma_\theta\right) \quad (6)$$

$$\dot{o}_r = A(r) + B(r)\cos(2\theta) + C(r)\sin(2\theta) \quad (7)$$

$$\begin{cases} A(r) = \dfrac{1-\nu^2}{E}\cdot\dfrac{\sigma_{xx}+\sigma_{yy}}{2}\left(1-\dfrac{R^2}{r^2}\right) \\ B(r) = \dfrac{1-\nu^2}{E}\cdot\dfrac{\sigma_{xx}-\sigma_{yy}}{2}\left(1+3\dfrac{R^4}{r^4}-4\dfrac{R^2}{r^2}\right) \\ C(r) = \dfrac{1-\nu^2}{E}\cdot\tau_{xy}\left(1+3\dfrac{R^4}{r^4}-4\dfrac{R^2}{r^2}\right) \end{cases} \quad (8)$$

For small deformation problems, the geometric equations that the surrounding rock of the tunnel must satisfy are given by Equation 9[23].

$$\dot{o}_r = \frac{\partial u_r}{\partial r} \quad (9)$$

Based on the relationship between strain and displacement, integration is performed.

$$u_r = \int \dot{o}_r dr = \int \left[A(r) + B(r)\cos(2\theta) + C(r)\sin(2\theta)\right]dr \quad (10)$$

$$\begin{cases} \int A(r)dr = \dfrac{1-\nu^2}{E}\cdot\dfrac{\sigma_{xx}+\sigma_{yy}}{2}\left(r+\dfrac{R^2}{r}\right) \\ \int B(r)dr = \dfrac{1-\nu^2}{E}\cdot\dfrac{\sigma_{xx}-\sigma_{yy}}{2}\left(r-\dfrac{R^4}{r^3}+4\dfrac{R^2}{r}\right) \\ \int C(r)dr = \dfrac{1-\nu^2}{E}\cdot\tau_{xy}\left(r-\dfrac{R^4}{r^3}+4\dfrac{R^2}{r}\right) \end{cases} \quad (11)$$

$$u_r = \frac{1-\nu^2}{E} r \left[\frac{\sigma_{xx}+\sigma_{yy}}{2}\left(1+\frac{R^2}{r^2}\right) + \frac{\sigma_{xx}-\sigma_{yy}}{2}\cos(2\theta)\left(1-\frac{R^4}{r^4}+\frac{4R^2}{r^2}\right) + \tau_{xy}\sin(2\theta)\left(1-\frac{R^4}{r^4}+\frac{4R^2}{r^2}\right)\right] \quad (12)$$

Unlu and Gercek[27] first observed that the LDP curves ahead of and behind the tunnel face do not follow a single continuous functional relationship with X. The monitoring cross-section can be divided into two states based on its position relative to the tunnel face, reflecting the spatial constraint effect of the tunnel excavation face[28]. At the tunnel face (X = 0), the radial displacement can be estimated using Poisson's ratio, where u^*_0 represents the displacement release factor at the tunnel face (X = 0).

When the distance approaches infinity, the displacement is expressed as shown in Equation 13:

$$u_{\max} = \lim_{r\to\infty} u_r = \frac{1-\nu^2}{E} r \left[\frac{\sigma_{xx}+\sigma_{yy}}{2} + \frac{\sigma_{xx}-\sigma_{yy}}{2}\cos(2\theta) + \tau_{xy}\sin(2\theta)\right] \quad (13)$$

When the monitoring section is located behind the excavation face, the displacement at the tunnel wall gradually increases as the distance from the face grows. After reaching a certain distance, the radial displacement stabilizes. This stabilized radial displacement can be regarded as the maximum displacement value u_{max}, within the range affected by the spatial effects of the excavation face. The longitudinal deformation curve is shown in Fig.4.

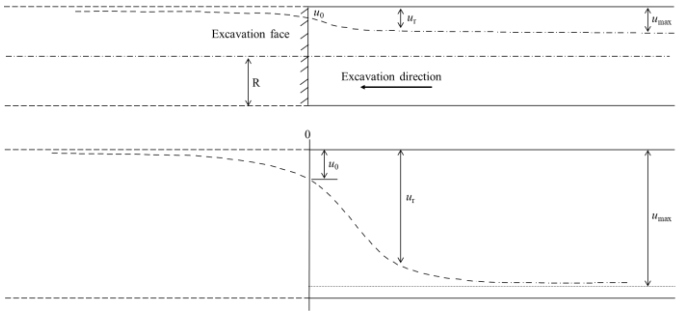


Fig. 4. Longitudinal deformation profile.

To characterize the LDP curves reflecting the spatial effect of the excavation face under different working conditions, the data needs to be normalized. Let $x^*=X/R$, representing the relative distance between the monitoring section and the excavation face (where X is the distance from the monitoring section to the excavation face; $X<0$ indicates the monitoring section is ahead of the face, and $X>0$ indicates it is behind the face; R is the excavation radius of the tunnel).

The extent of surrounding rock displacement release is described by the displacement release factor u^*, defined as the ratio of the radial displacement u^* at the tunnel wall to its maximum displacement u_{max} under plane strain conditions without support. That is:

$$u^* = \frac{u_r}{u_{\max}} \quad (14)$$

2.2 Numerical model scheme

This numerical simulation is based on the modeling approach of "Rhino^{3D}-Griddle-Flac^{3D}." Utilizing Rhino^{3D}-FLAC^{3D} coupling technology, a three-dimensional inclined shaft tunnel model was established. The model's element structure consists of unstructured elements, including hexahedrons, tetrahedrons, and triangular prisms[29]. By importing the model generated in Rhino into the FLAC^{3D} software[30], the limitations of FLAC^{3D}'s pre-processing capabilities were circumvented. Particularly in meeting the requirements for various mesh element types, this method improved computational speed while ensuring accuracy[31-32]. The Mohr-Coulomb model was adopted for the rock mass constitutive model. This model employs a simplified geological model for analysis, aiming to reveal the influence of different parameters on the LDP curve. The tunnel radius is R = 3.8 meters. Since selecting an influence zone of 3–5 times the excavation size is considered most reasonable, and to balance solution accuracy with computational speed, a region of 76 m × 60 m × 76 m (width × length × height) was chosen to establish the FLAC^{3D} calculation model. The model is divided into a total of 73,888 nodes and 114,077 elements. The model mesh and geometry are shown in Fig.5.

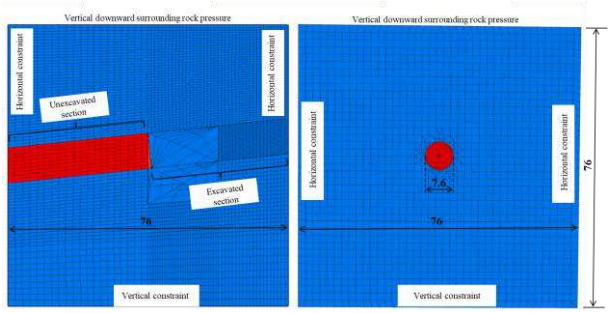


Fig. 5. Model mesh and geometry diagram

Displacement constraints are applied at the bottom and both side boundaries of the model, while a uniform load equivalent to the self-weight of the overlying surrounding rock is applied to the upper boundary. The initial in-situ stresses in the formation include vertical stress σ_y and horizontal stresses σ_x and σ_z, which are calculated according to the following formulas:

$$\sigma_y = \sigma_0 + \sum \gamma_i h_i \tag{15}$$

$$\sigma_x = \sigma_z = \lambda \sigma_y \tag{16}$$

Where γ_i is the unit weight of the overlying rock in each layer, kN·m^{-3}; h_i is the thickness of the overlying rock in each layer, m; and λ is the lateral pressure coefficient. In this study, to investigate the longitudinal deformation profile of circular tunnels under a three-dimensional stress field, the control variable method is employed. Different working condition schemes are established to analyze the displacement evolution patterns of inclined shaft tunnels. Based on setting the horizontal lateral pressure coefficient λ_H, the axial lateral pressure coefficient λ_h is introduced, where $\lambda_H=\sigma_y/\sigma_z$ and $\lambda_h=\sigma_x/\sigma_z$. When the tunnel is in a stress environment at a burial depth of 600 m, certain mechanical parameters of the surrounding rock of the circular tunnel

are assumed: σ_z = 15 MPa, tunnel radius R = 3.8 m, inclination angle of the inclined shaft α= 5°, angle between the shaft axis and the projection of σ_h onto the plane of the circular inclined shaft β = 0°, elastic modulus E = 10 GPa, Poisson's ratio υ = 0.2, cohesion c = 3 MPa, and internal friction angle φ = 25°.

Table 1 Numerical Simulation Schemes

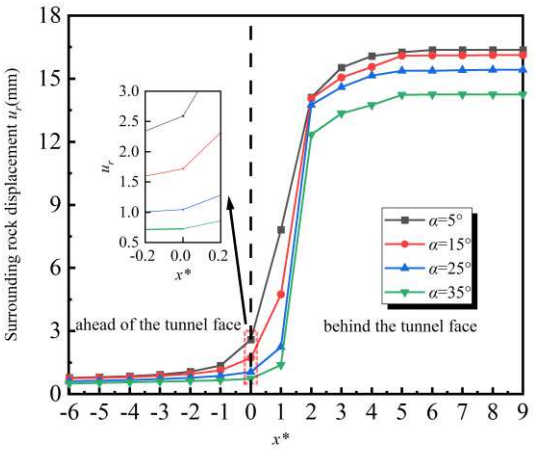
Geological structural factor α (°)	Geological structural factor β (°)	Axial lateral pressure coefficient λ_h	Horizontal lateral pressure coefficient λ_H	Elastic modulus E/GPa	Poisson's ratio v	Cohesion c (MPa)	Internal friction angle φ (°)
5	0	0.5	0.5	5	0.2	2	20
15	30	0.75	0.75	10	0.25	3	25
25	60	1	1	15	0.3	2.5	30
35	90	1.25	1.25	20	0.35	3.5	35

Table 1 presents the numerical simulation schemes, which consider a total of 8 influencing parameters. The observation plane is set at the center cross-section, i.e., at 30 m. Excavation advances with a step length of 1.5 m each time, progressing to the observation plane over 20 excavation steps. Radial displacement monitoring points on the tunnel wall are established every 3.8 m.

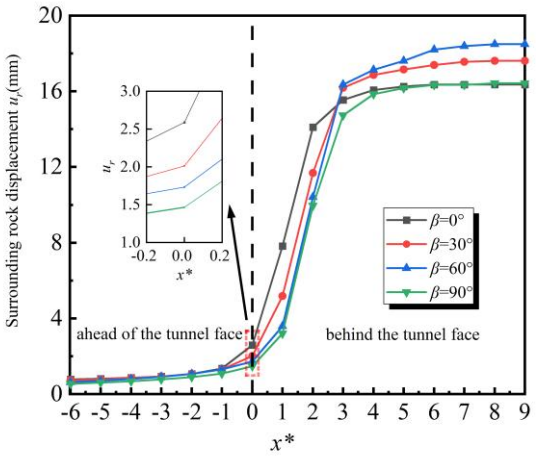
3 Influence patterns of typical factors

3.1 Influence of geological structural factors on displacement and displacement release coefficient

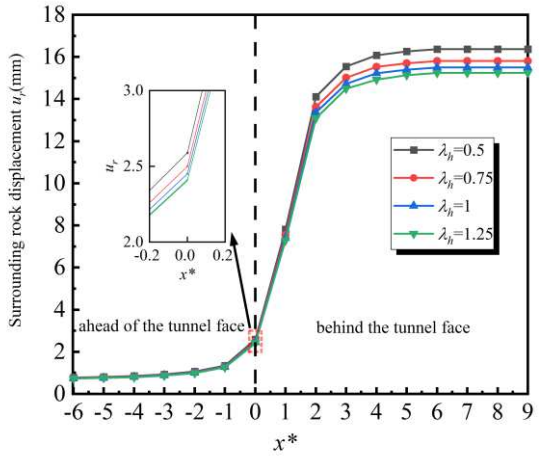
Select typical geological structural factors such as α, β, the axial lateral pressure coefficient, and the horizontal lateral pressure coefficient, and analyze their impact patterns on the longitudinal deformation characteristics of surrounding rock. The longitudinal deformation curve of the surrounding rock is illustrated in Fig.6.



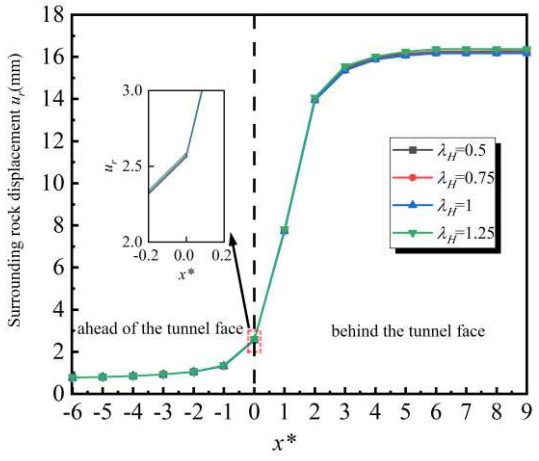
(a) α



(b) β



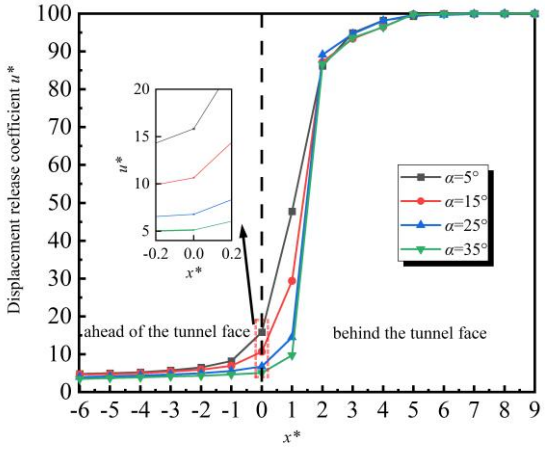
(c) λ_h



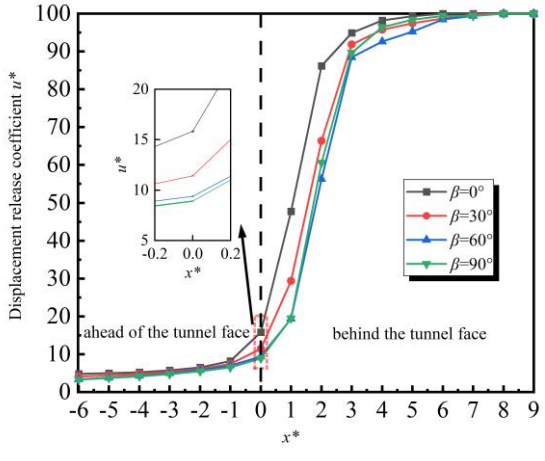
(d) λ_H

Fig. 6 Geological structural factors influencing the deformation of surrounding rock

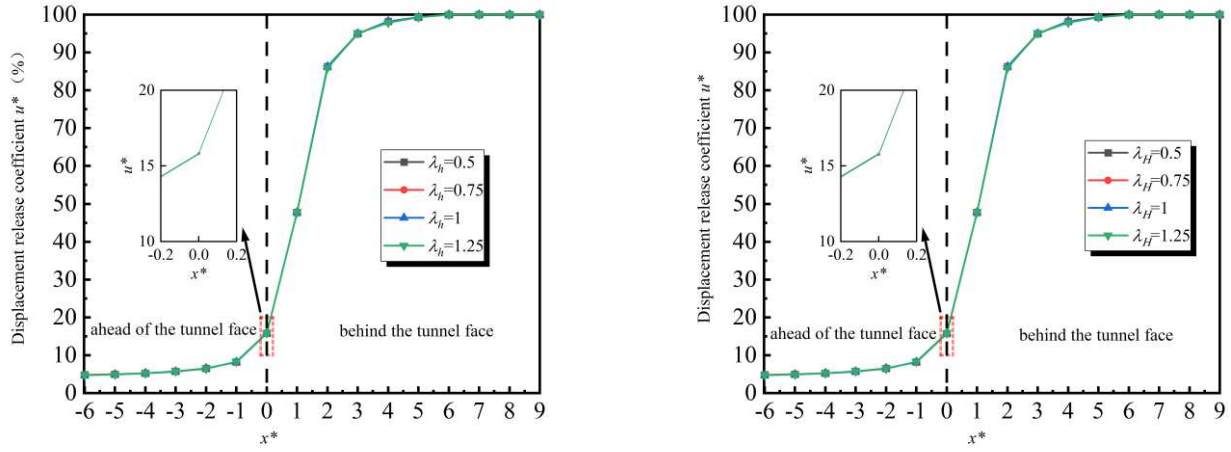
Fig.6 reveals the differential influence patterns of different geo-mechanical parameters on the radial displacement of surrounding rock in the inclined shaft. Regarding the effect of the spatial inclination angle α, as α increases from 5° to 35°, the maximum radial displacement of the surrounding rock gradually decreases from 16.367 mm to 14.256 mm, indicating that a larger inclination angle can effectively inhibit surrounding rock deformation. The influence of the orientation angle β exhibits a nonlinear characteristic: when β increases from 0° to 60°, the displacement rises from 16.367 mm to a peak of 18.490 mm; as β further increases to 90°, the displacement then decreases to 16.434 mm, demonstrating the sensitivity of surrounding rock deformation to the tunnel's orientation. In terms of the stress environment, an increase in the axial lateral pressure coefficient causes the displacement to steadily decrease from 16.367 mm to 15.239 mm, reflecting its significant constraining effect. In contrast, variations in the horizontal lateral pressure coefficient only induce minor fluctuations between 16.172 mm and 16.367 mm, indicating its relatively limited control over surrounding rock deformation.



(a) α



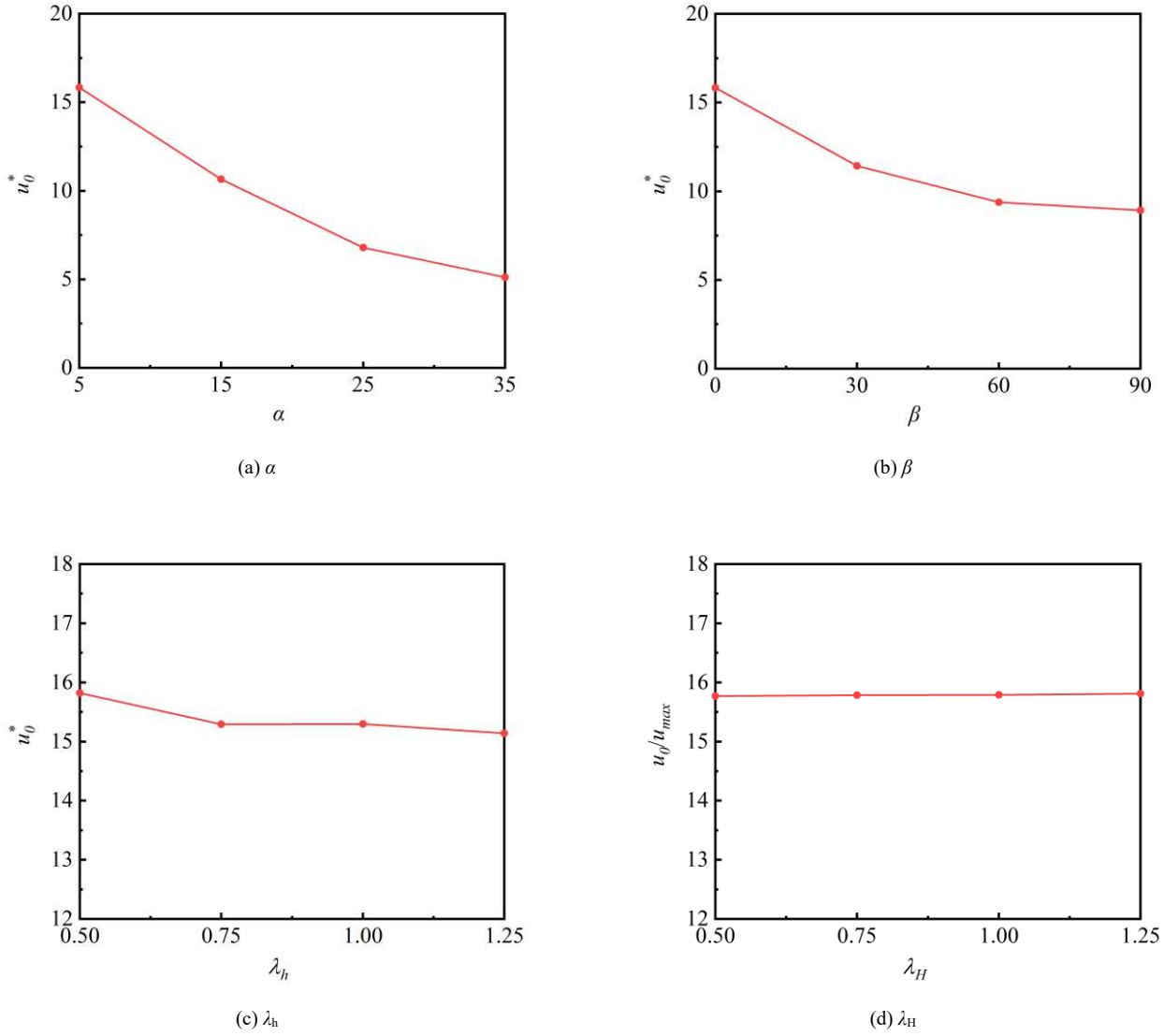
(b) β



(c) λ_h (d) λ_H

Fig. 7 Impact of geological structural factors on displacement release coefficient

Fig 7 provides an in-depth illustration of the controlling mechanisms of geological structural factors on the evolution of the displacement release coefficient. The increase in the spatial parameter α significantly alters the development path of surrounding rock deformation. When α is 5°, the displacement release coefficient increases from 8.24% ahead of the tunnel face to 86.18% behind it, while when α rises to 25°, the variation range shifts to 5.59%–89.19%. Its influence zone remains stable within the interval of X/R = −6 to 6. The parameter β exhibits more complex spatial effects. As β increases from 0° to 60°, the variation amplitude of the displacement release coefficient narrows from 86.18% to 56.31%, and the affected zone expands to a larger interval of X/R = −6 to 9. This indicates that the relative orientation between the tunnel axis and the principal stress direction substantially adjusts the spatial effect domain. In contrast to conventional understanding, variations in the axial and horizontal lateral pressure coefficients have relatively limited influence. Under different working conditions, the abrupt change amplitude of the displacement release coefficient remains within a small fluctuation range of 85.4% to 86.6%, and all curves maintain the typical S-shaped evolutionary pattern. In all cases, a sudden increase in the displacement release coefficient is observed as the tunnel face is traversed. This nonlinear jump characteristic reveals the abrupt release of the spatial constraint effect induced by excavation. The differences in curve morphology under different parameters reflect the intrinsic mechanism by which geological structural factors regulate the spatiotemporal development of surrounding rock deformation through modifications in the three-dimensional stress field.



(a) α (b) β

(c) λ_h (d) λ_H

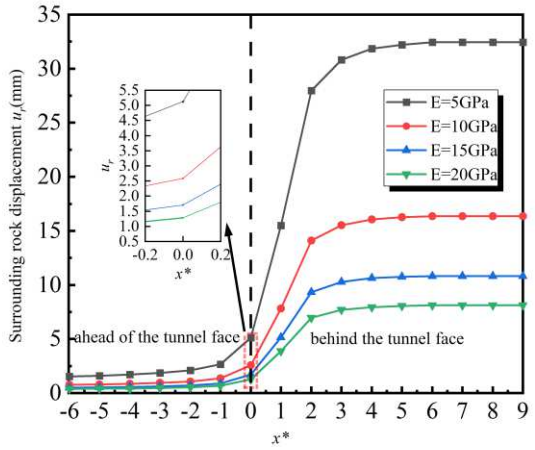
Fig. 8 Variation of displacement release coefficient at tunnel face

Fig. 8 clearly illustrates the variation pattern of the displacement release coefficient at the tunnel face with different geological structural factors, profoundly revealing the dominant role of spatial parameters compared to traditional stress parameters. Analysis shows that the spatial parameter α has an extremely significant influence on the displacement release coefficient at the tunnel face. When α increases from 5° to 35°, the displacement release coefficient sharply decreases from 15.830% to 5.107%. This is primarily because an increase in α reduces the component of vertical stress on the inclined shaft plane, thereby weakening the initial deformation tendency of the surrounding rock near the tunnel face. Similarly, the spatial parameter β also exhibits crucial influence. As β varies from 0° to 90°, the displacement release coefficient decreases from 15.830% to 8.920%, reflecting that changes in the relative orientation between the tunnel axis and the in-situ stress field significantly alter the mechanical response of the surrounding rock at the tunnel face. It can be seen from the figure that variations in the axial lateral pressure coefficient and the horizontal lateral pressure coefficient have a negligible impact on the displacement release coefficient at the tunnel face. When the axial lateral pressure coefficient varies between 0.5 and 1.25, the displacement release

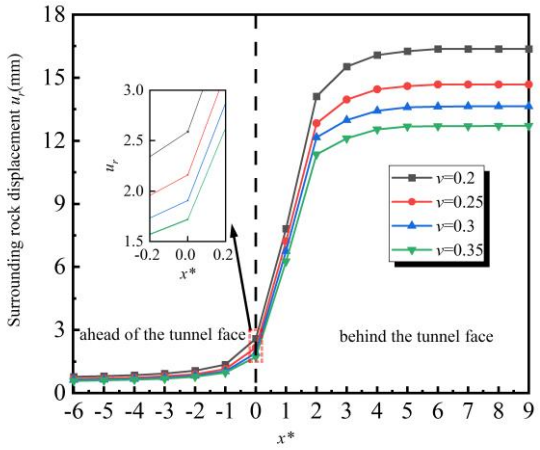
coefficient fluctuates only within a narrow range of 15.141% to 15.823%. The influence of the horizontal lateral pressure coefficient is similarly limited, with the variation range of the displacement release coefficient caused by its change being only 15.772% to 15.808%. This comparison strongly confirms that in three-dimensional spatial problems such as those encountered in inclined shafts or tunnels, the key factor determining the strength of spatial effects at the tunnel face lies in the spatial geometric orientation of the tunnel, rather than traditional stress magnitude parameters. This finding holds significant guiding importance for engineering practice, indicating that in the support design for inclined shafts, precise assessment and control of the tunnel's spatial orientation must be prioritized.

3.2 Influence of mechanical parameters of surrounding rock on displacement and displacement release coefficient

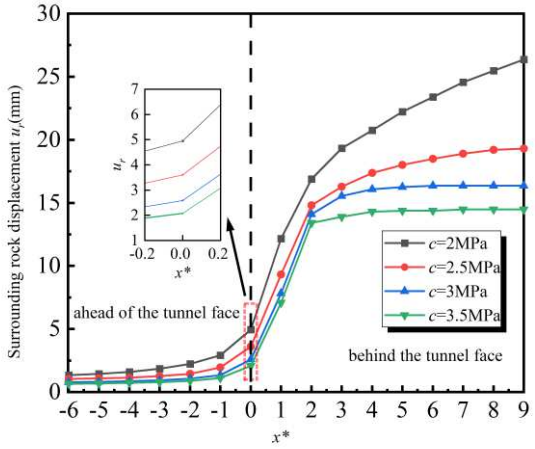
Select elastic modulus, Poisson's ratio, cohesion, and internal friction angle as mechanical properties, and analyze their influence patterns on the longitudinal deformation characteristics of surrounding rock. The longitudinal deformation curve of the surrounding rock is shown in Fig.9.

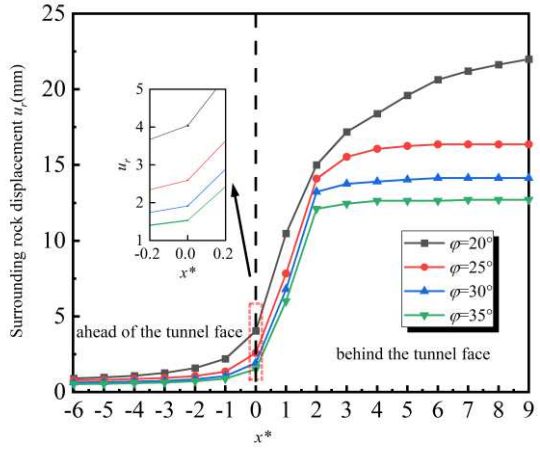


(a) E



(b) v



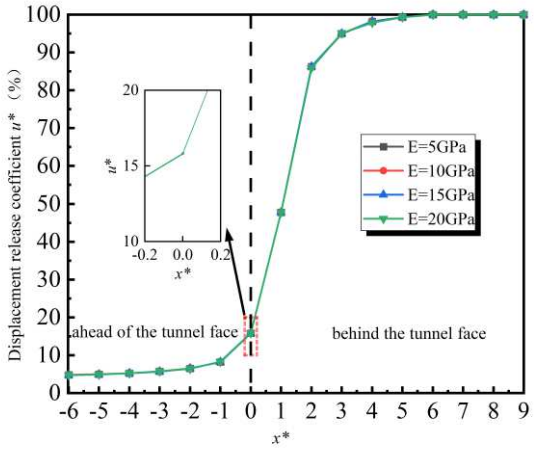


(c) c (d) φ

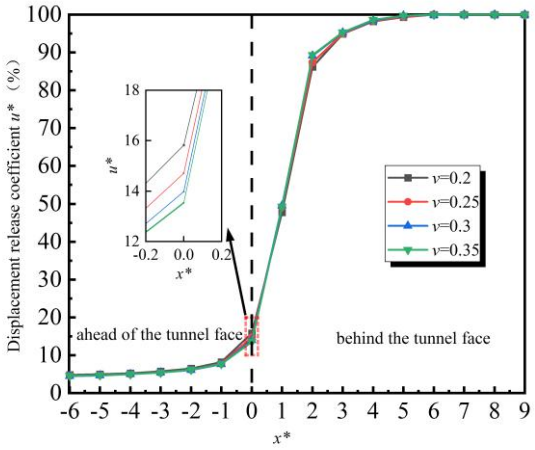
Fig. 9 Influence of different mechanical parameters on surrounding rock deformation

Fig.9 systematically reveals the controlling mechanism of the mechanical properties of surrounding rock on tunnel deformation behavior, clearly demonstrating the differential influence patterns of various parameters on displacement development. The variation in elastic modulus significantly alters the deformation scale of the surrounding rock. When the elastic modulus increases from 5 GPa to 20 GPa, the maximum radial displacement substantially decreases from 32.443 mm to 8.111 mm, exhibiting a typical inverse proportional relationship. This fully demonstrates the fundamental role of rock mass stiffness in resisting deformation. The increase of Poisson's ratio within the range of 0.2 to 0.35 also leads to a reduction in displacement, from 16.367 mm to 12.705 mm. This phenomenon is closely related to the change in axial stiffness caused by the enhanced lateral deformation capacity of the rock mass. The strength parameters of the rock mass exhibit more complex controlling characteristics. When cohesion increases from 2 MPa to 3.5 MPa, the displacement decreases from 26.379 mm to 14.470 mm, a reduction of 45.2%. As the internal friction angle increases from 20° to 35°, the displacement decreases from 21.993 mm to 12.702 mm, a reduction of 42.3%. The significant influence of these two strength parameters highlights the critical role of rock mass shear strength in controlling surrounding rock deformation. It is particularly noteworthy that when the cohesion is 2 MPa, the surrounding rock fails to reach a stable deformation state, indicating that under this strength condition, the surrounding rock may have entered a stage of plastic development. This phenomenon carries important warning significance for the timing selection of engineering support.

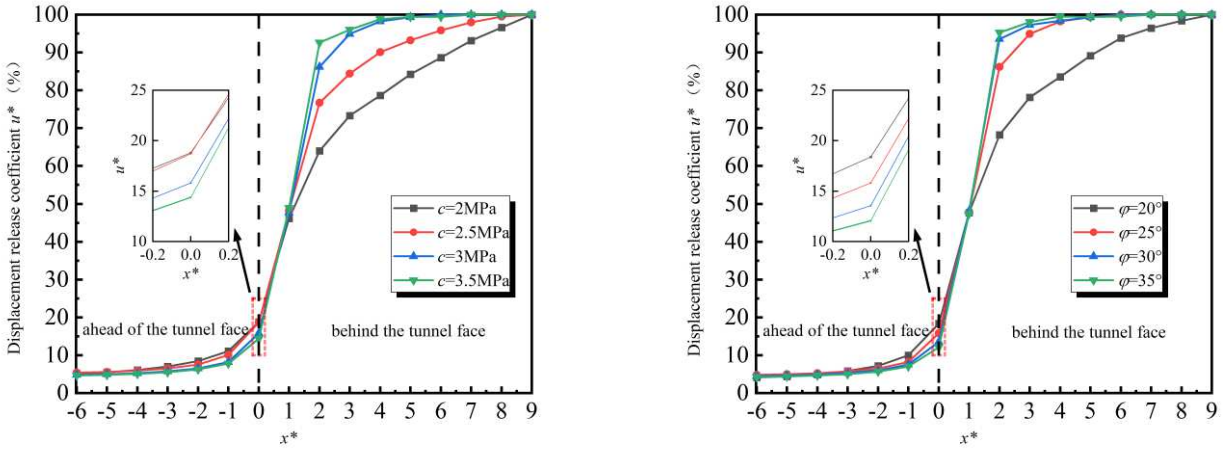
By comparing the magnitude of influence of the four parameter groups, it can be found that the elastic modulus variation causes the largest displacement difference. Although the influence of strength parameters is relatively smaller, their characteristics near critical states are more pronounced. These patterns collectively indicate that in inclined shaft or tunnel engineering, accurately obtaining the mechanical parameters of the rock mass and identifying their dominant control mechanisms play a decisive role in predicting surrounding rock deformation behavior and formulating reasonable support schemes.



(a) E



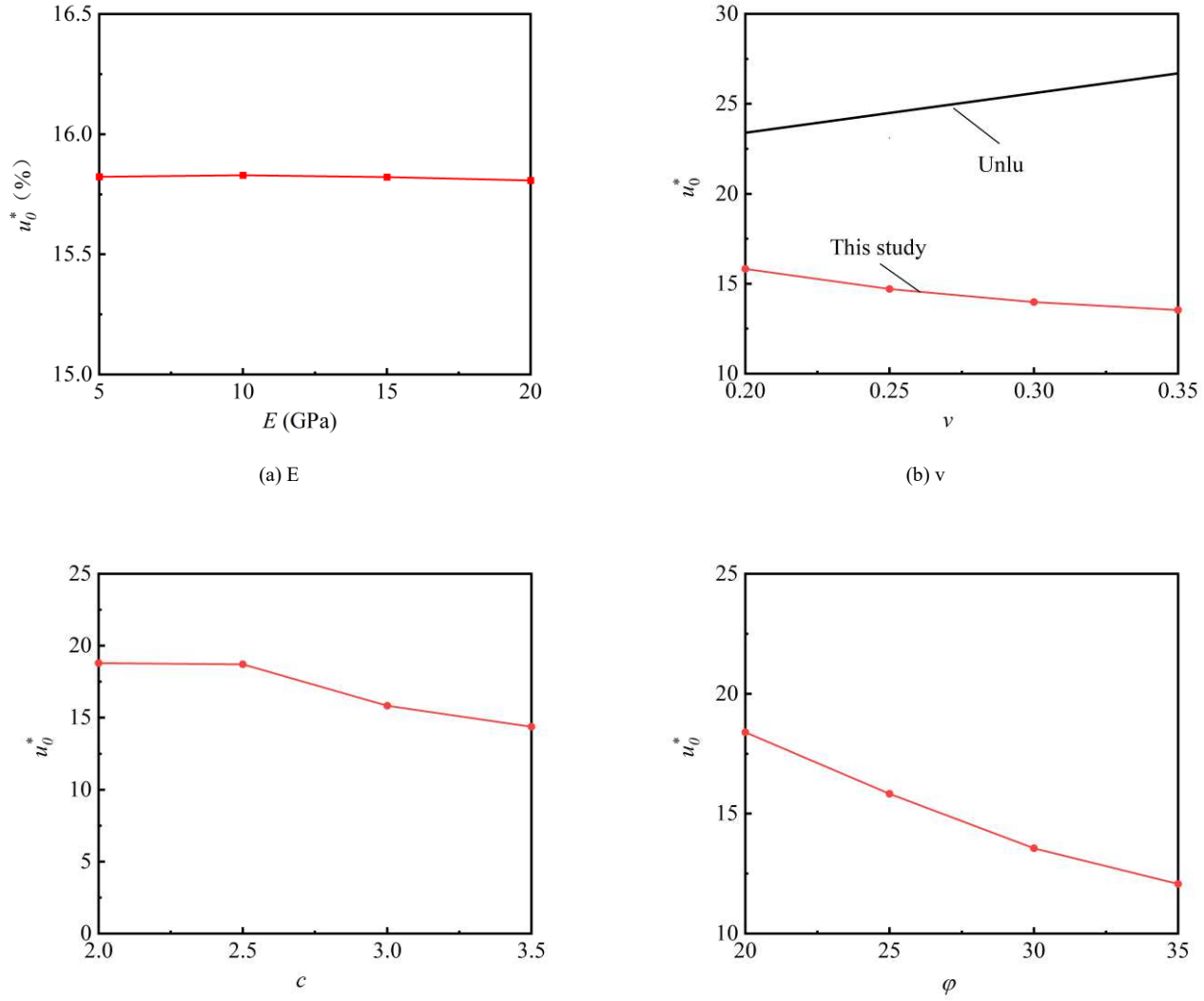
(b) v



(c) c (d) φ

Fig. 10 Influence of different geological factors on the displacement release coefficient

The data in Fig.10 reveals the differential influence of different mechanical parameters on the spatial distribution pattern of the displacement release coefficient. Variations in the elastic modulus do not alter the fundamental distribution characteristics of the displacement release coefficient. The curves under all scenarios maintain a complete "S"-shaped evolution pattern. The displacement release coefficient at the tunnel face remains within a narrow range of 8.24% to 8.26%, while the far-field value ranges between 85.91% and 86.25%. This indicates that material stiffness primarily controls the magnitude of absolute displacement, with minimal impact on the spatial distribution pattern of the dimensionless displacement release coefficient. The effect of Poisson's ratio exhibits distinct spatial locality, with its influence confined to a region within approximately 3 times the tunnel diameter in front of and behind the tunnel face. As Poisson's ratio increases from 0.2 to 0.35, the displacement release coefficient at the tunnel face gradually changes from 8.24% to 7.72%, while the far-field value increases from 86.18% to 89.32%. This non-synchronous response between the near-field and far-field reflects the modulating effect of rock mass deformation properties on the propagation process of spatial effects. The strength parameters demonstrate significant control over the curve morphology and development process. When cohesion is 2 MPa, the curve form is incomplete. After increasing to 3.5 MPa, not only does the release coefficient at the tunnel face decrease from 11.10% to 7.81%, but a complete "S"-shaped curve is also formed. The influence of the internal friction angle is more systematic. As it increases from 20° to 35°, the release coefficient at the tunnel face decreases from 9.99% to 7.04%, and the far-field value substantially increases from 68.23% to 95.27%. These characteristics fully demonstrate that the rock mass strength parameters are the dominant factors controlling the spatiotemporal evolution characteristics of the displacement release coefficient.



(a) E (b) v

(c) c (d) φ

Fig. 11 Influence of different geological factors on the displacement release coefficient at the tunnel face

Fig.11(a) illustrates the relationship between the tunnel face displacement release coefficient u^*_0 and the elastic modulus E. As the elastic modulus increases from 5 GPa to 20 GPa, the tunnel face displacement release coefficient remains within an extremely narrow fluctuation range of 15.82% to 15.83%. This nearly constant characteristic indicates that material stiffness has a negligible effect on the dimensionless displacement release coefficient, with its primary role being the control of the absolute displacement value.

Fig.11(b) shows the relationship between the tunnel face displacement release coefficient u^*_0 and Poisson's ratio v. Near the observation face, the surrounding rock displacement release coefficient varies under different Poisson's ratio conditions. As Poisson's ratio increases from 0.2 to 0.35, the tunnel face displacement release coefficient decreases linearly from 15.83% to 13.54%. Based on the numerical simulation results, the relationship between the tunnel face displacement release coefficient u^*_0 and Poisson's ratio v is fitted, yielding the displacement release coefficient u^*_0 for the inclined shaft circular tunnel face as:

$$u_0^* = -0.15v + 0.10 \quad (18)$$

Meanwhile, the fitting formula provided by Unlu and Gercek[27] is as follows.

$$u_0^* = 0.22v + 0.19 \quad (19)$$

An error analysis of the fitting results was conducted: the root mean square error RMSE=5.816×10^{-2}, the sum of squared errors SSE=1.1632×10^{-1}, the correlation coefficient R = 0.9803, and the coefficient of determination DC = 0.961. The fitting results are reliable. Based on the formula, it can be concluded that for inclined shaft tunnels under the same conditions, a larger Poisson's ratio of the surrounding rock leads to a smaller displacement release coefficient at the same position relative to the tunnel face. Comparing the fitting results with the formula provided by Unlu and Gercek reveals that the intercept and slope are smaller. Compared to horizontal tunnels, the longitudinal deformation curve of inclined shafts is less affected by Poisson's ratio. Although the potential influence range may be relatively narrow, its presence suggests that some unexplained phenomena are affecting the value of u^*_0.

As shown in Fig.11(c) and (d), when cohesion increases from 2 MPa to 3.5 MPa, the release coefficient decreases from 18.80% to 14.38%. Similarly, as the internal friction angle rises from 20° to 35°, the release coefficient drops from 18.40% to 12.08%. This trend indicates that shear strength parameters of the rock mass influence spatial effects by controlling the development range of the plastic zone in the surrounding rock. When the strength parameters are low, the plastic zone ahead of the tunnel face expands, leading to greater deformation release before support is applied. In contrast, increased strength effectively restricts the expansion of the plastic zone, concentrating deformation more behind the tunnel face. This mechanism demonstrates that strength parameters exert a more fundamental control over the spatial effects in inclined tunnels compared to deformation parameters.

4 Verification of modified LDP fitting formula

4.1 Modified LDP fitting formula

According to literature[27], the curves ahead of and behind the observation face do not follow a single continuous functional relationship with X. When the monitoring face is located ahead of the tunnel face, X < 0, theoretically, as X → ∞, the displacement release coefficient $u^* = 0$, and $A_a = -u^*_0$.

$$\lim_{X\to\infty} u^* = 0, u_0^* = -A_a \quad (20)$$

When the monitoring face is located behind the tunnel face, X > 0, theoretically, as X → ∞, the displacement release coefficient $u^* = 1$, and $A_b = 1 - u^*_0$.

$$\lim_{X\to\infty} u^* = 1, u_0^* = 1 - A_b \quad (21)$$

It has been found that the statistical constants B_a and B_b are both linearly related to Poisson's ratio B_b. Through statistical analysis and fitting, the following equations are obtained:

$$\begin{cases} B_a = 1.2111675\nu - 0.110345 \\ B_b = 1.108385\nu + 0.3365975 \end{cases} \quad (22)$$

Combined with equation 14, the modified formula for the longitudinal deformation curve of the inclined shaft roadway is derived as follows:

$$\begin{cases} u_0^* = 0.09018\nu + 0.07826 (X=0) \\ u^* = u_0^* + A_a[1 - e^{(B_a x^*)}] (X<0) \\ u^* = u_0^* + A_b\{1 - [B_b/(B_b + x^*)]^2\} (X>0) \end{cases}$$
$$(A_a = -0.09018\nu - 0.07826,\ B_a = 1.2111675\nu - 0.110345, \quad (23)$$
$$A_b = -0.09018\nu + 0.92174,\ B_b = 1.108385\nu + 0.3365975)$$

The spatial parameters α and β cause changes in the local stress direction, which in turn leads to an adjustment in the lateral pressure coefficient λ. If α increases, the component of vertical stress σ_v on the inclined shaft plane decreases, while the component of horizontal stress σ_h increases, resulting in an increase in λ. To facilitate the study, an equivalent lateral pressure coefficient λ' is introduced. The equivalent lateral pressure coefficient can be defined as the ratio of the average horizontal stress to the vertical stress. From (Equation 1), it can be seen that:

$$\lambda' = \frac{\sigma_H + \sigma_h \cos^2\alpha + \sigma_v \sin^2\alpha}{2(\sigma_h \sin^2\alpha + \sigma_v \cos^2\alpha)} \quad (24)$$

Substituting (16) into the expression yields:

$$\lambda' = \frac{\lambda(1 + \cos^2\alpha) + \sin^2\alpha}{2(\lambda \sin^2\alpha + \cos^2\alpha)} \quad (25)$$

When the monitoring face is located ahead of the tunnel face (X<0), the exponential function $1\text{-}e^{Ba\ x^*}$ describes the displacement release rate. A larger Ba value corresponds to a faster displacement release. The tunnel crown, being significantly influenced by gravity, exhibits a wide displacement release range (X/R = -4 ~ 7). To allow displacement to release more rapidly ahead of the tunnel face, a crown adjustment factor $\gamma(\lambda')=1+c_1\lambda'$ is introduced.

$$\begin{cases} u_0^* = (0.08119\nu + 0.43927)\cdot \mathrm{f}(\lambda') (X=0) \\ u^* = u_0^* + A_a[1 - e^{(B_a x^*)}] (X<0) \\ u^* = u_0^* + A_b\{1 - [B_b/(B_b + x^*)]^2\} (X>0) \end{cases}$$
$$(A_a = -(0.08119\nu + 0.43927)\cdot \mathrm{f}(\lambda'),\ B_a = (1.2111675\nu - 0.110345)\cdot \gamma(\lambda'), \quad (26)$$
$$A_b = -(0.08119\nu - 0.56073)\cdot \mathrm{f}(\lambda'),\ B_b = (1.108385\nu + 0.3365975)\cdot \delta(\lambda'),$$
$$\mathrm{f}(\lambda') = 1 + C(\lambda' - 1),\ \gamma(\lambda') = 1 + \mathrm{c}_1\lambda',\ \delta(\lambda') = 1 + \mathrm{c}_2\lambda')$$

4.2 Engineering verification

To verify the above formula, the inclined shaft of Shenhua Xinjie Coal Mine in Ordos City, Inner Mongolia Autonomous Region, was selected for study. The mining area is located in the south-central part of the Ordos Plateau. The first layer is the surface layer, primarily consisting of aeolian sand, with a thickness of less than 10 meters. The second layer is the Lower Cretaceous Zhidan Group (K_1zh), with an average thickness of 376 meters. The lithology of this stratum is mainly composed of brownish-red and purplish-brown medium to fine-grained sandstones. The third layer is the Middle Jurassic Anding Formation (J_2a), with an average thickness of 120 meters. The lithology of this stratum is primarily purplish-brown or brownish-red fine to coarse-grained sandstones. The fourth layer is the Middle Jurassic Zhiluo Formation (J_2z), with an average thickness of 143 meters. The lithological combination of this stratum consists of gray-green sandy mudstone in the upper part and gray-green medium sandstone in the lower part. The fifth layer is the Middle Jurassic Yan'an Formation ($J_{1-2}y$), with an average thickness of 50 meters. This formation is mainly composed of gray-white medium-grained sandstone. No faults, folds, or intrusive igneous rocks were found within the survey area, indicating that the geological structure is of a simple type. The geological profile is shown in Fig.12, and the physical and mechanical parameters of the rock layers are listed in Table 2.

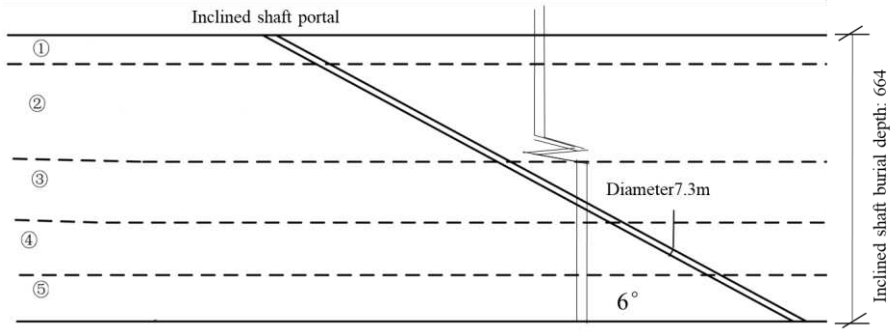


Fig. 12 Geological cross-section

Table 2 Physical and mechanical parameters of rock strata

Rock Type	Average Unit Weight /(kN·m^{-3})	Elastic Modulus /GPa	Poisson's Ratio	Internal Friction Angle /(°)	Cohesion /MPa	Tensile Strength /MPa
②Lower Cretaceous Zhidan Group K_{1zh}	24.9	7.3	0.21	27.2	2.6	0.74
③Jurassic Anding Formation J_{2a}	24.7	9.6	0.20	27.1	2.9	0.98
④Jurassic Zhiluo Formation J_{2z}	25.0	10.8	0.20	27.2	3.2	1.07
⑤Jurassic Yan'an Formation J_{1-2y}	25.1	8.5	0.17	27.1	3.3	1.72

Fig.13 shows the displacement release coefficient curve and the envelope. It can be seen from Fig.13 that within the range influenced by the spatial effects of the excavation face in the inclined shaft, the LDP curves for each working condition are clustered near the average value. Therefore, for specific projects, it is recommended to obtain the LDP curve and u_{max} through numerical calculation methods. The design of support parameters should then be carried out by considering the influence of spatial parameters α, β, and rock property parameters v, c, φ, with the aid of the envelope and the corresponding average values.

The consistency and accuracy of the proposed analytical model can be validated by leveraging the LDP expression from previous studies and numerical simulation results[28]. Representative formulas are listed in Table 3.

Table 3 Representative formulas

Formula	Expression	Influencing Factors
Panet	$u^* = 0.25 + 0.75\left[1 - \left(\frac{0.75}{0.75 + x^*}\right)^2\right]\ (X \geq 0)$	x^*（X/R）
Hoek	$u^* = \left[1 + exp\left(-\frac{x^*}{1.10}\right)\right]^{-1.7}$	x^*（X/R）
Unlu and Gercek	$\begin{cases} u_0^* = 0.22\nu + 0.19 (X=0) \\ u^* = u_0^* + A_a[1 - e^{(B_a x^*)}] (X<0) \\ u^* = u_0^* + A_b\{1 - [B_b/(B_b + x^*)]^2\} (X>0) \end{cases}$ ($A_a = -0.22\nu - 0.19$，$B_a = 0.73\nu + 0.81$，$A_b = -0.22\nu + 0.81$，$B_b = 0.39\nu + 0.65$)	x^*（X/R），ν

Fig.14 presents a comparison with existing formulas. The modified LDP fitting formula shows good overall agreement with the FLAC3D calculation results obtained in this study, with some discrepancies possibly attributed to mesh precision. By comparing the calculation results with the displacement release coefficients proposed by other scholars, it can be observed that the modified fitting curve in this study, which considers the influence of spatial parameters α, β, and lithological parameters ν, c, φ on the spatial effects of the excavation face in inclined circular shafts, aligns well with the numerical simulation results under actual working conditions. This demonstrates the reliability of the fitting formula proposed in this study. However, existing formulas, which do not account for the conditions of spatial parameters α, β, and lithological parameters ν, c, φ for horizontal tunnels, show slight deviations from the fitting formula presented here. Analysis indicates that during the excavation of inclined shafts, the in-situ stress on the surrounding rock ahead of the excavation face gradually increases. This means that the same location in the unexcavated surrounding rock bears a greater load, causing the roof of this section to deform earlier during excavation, resulting in a larger influence range ahead of the excavation face. In contrast, the stress released in the excavated surrounding rock is smaller than that released at the same location in horizontal tunnels. Therefore, the rate of deformation release in the roof of the surrounding rock after excavation is slower compared to horizontal tunnels, leading to a slightly larger influence range behind the excavation face. Thus, the modified fitting formula proposed in this study can better reflect the spatial effect patterns of inclined shafts under three-dimensional spatial conditions, ensuring the safety and scientific rationality of inclined shaft support.

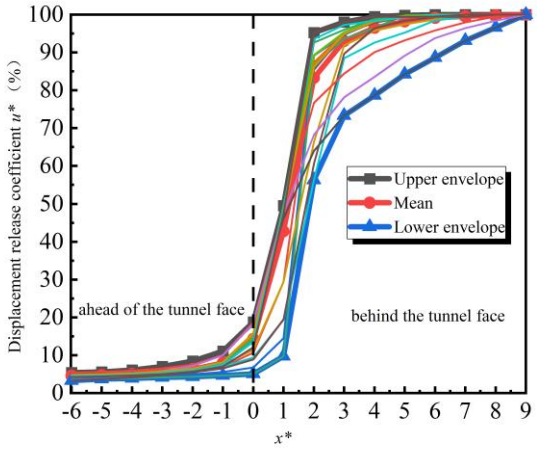


Fig. 13 Displacement Release Coefficient Curve and Envelope Line

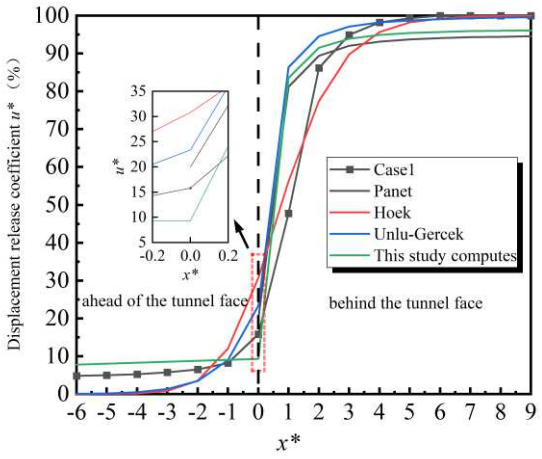


Fig.14 Comparison Diagram with Existing Formulas

5 Conclusion

This study establishes the corresponding longitudinal deformation and displacement release coefficient curves of surrounding rock for circular inclined shafts in three-dimensional space. It investigates the influence of the coupling between spatial parameters and rock property parameters on the surrounding rock release coefficient and its evolution process. Additionally, the Unlu-Gercek formula is modified based on the main influencing factors, resulting in a fitted formula for the surrounding rock release coefficient of circular inclined shafts. The following conclusions are drawn:

(1) Geological structural factors α and β, as well as mechanical parameters cohesion and internal friction angle, have a significant influence on the shape of the LDP curve. The influence range of α on the LDP curve shape is between X/R = -6 and 6, while the influence ranges of β, cohesion, and internal friction angle are between X/R = -6 and 9. These parameters should be given priority during support parameter design.

(2) The axial lateral pressure coefficient, horizontal lateral pressure coefficient, and elastic modulus have a relatively minor

394 influence on the shape of the LDP curve. The convergence displacement and maximum displacement at various points along the
395 tunnel wall decrease proportionally as the elastic modulus increases, resulting in a constant displacement release coefficient
396 despite these changes. Thus, their effect on the displacement release coefficient at the excavation face can be neglected. The
397 influence of Poisson's ratio on the displacement release coefficient is mainly concentrated near the excavation face, with an
398 effective range on the LDP curve shape between X/R = -1 and 3. Its effect on the displacement release coefficient at the
399 excavation face is small but not negligible.

400 (3) For specific engineering projects, it is recommended to use numerical calculation methods to obtain the LDP curve and
401 u_{max}. Support parameter design should be conducted by considering the influence of geological structural factors α and β, along
402 with mechanical parameters v, c, and φ, utilizing envelope curves and their corresponding average values. The modified fitting
403 formula proposed in this study can better reflect the spatial effect laws of inclined shaft tunnels under three-dimensional
404 conditions, thereby ensuring the safety and scientific soundness of inclined shaft support.

References

Hou, G. Y., Liang, J. P., & Li, X. R. (2022). Research on principles and methods of roadway support design under conventional conditions. Chinese Journal of Rock Mechanics and Engineering, 41(4), 691-711.

Song F , Rodriguez-Dono A , Olivella S ,et al.Analysis and modelling of longitudinal deformation profiles of tunnels excavated in strain-softening time-dependent rock masses[J].Computers and Geotechnics, 2020.

Wang, J. C., Meng, L. Z., Zhang, D. L., et al. (2025). Evolution Law of Longitudinal Deformation Curve and Release Coefficient of Viscoelastic Rock. Journal of Shanghai Jiaotong University, 59(4), 513-524.

Ren, Z. J., Wang, T., Wu, S. C., et al. (2024). Stability analysis and application of soft rock tunnels based on Hoek-Brown strength criterion. Chinese Journal of Rock Mechanics and Engineering, 43(Suppl. 2), 3779-3791.

Yu, Y. J., Zhang, L., Song, Z. R., et al. (2023). Effects of excavation and support schemes on stability of surrounding rock of tunnels. Chinese Journal of Geotechnical Engineering, 45(Suppl. 2), 284-287.

Wang J ,Li E ,Chen L , et al. Measurement and analysis of the internal displacement and spatial effect due to tunnel excavation in hard rock[J].Tunnelling and Underground Space Technology incorporating Trenchless Technology Research,2019,84151-165.

Li G , Sun Q , Ma F,et al. Damage evolution mechanism and deformation failure properties of a roadway in deep inclined rock strata[J].Engineering failure analysis, 2023.

Chen L , Liu Y , He G ,et al. Study of longitudinal deformation profiles in high-ground-stress mega-section tunnels based on the Hoek–Brown criterion[J].Structures, 2024, 61.

Sun Wang. Study on Longitudinal Displacement Profiles of Tunnels Based on the Hoek-Brown Failure Criterion[D]. Hunan University, 2017.

Liang, Y.-W., Zha, W.-H., Wu, B., et al. (2023). Estimation of initial support time of soft rock tunnel based on convergence constraint method—Take Fengkeng Tunnel of Yiyong Highway as an example. Science Technology and Engineering, 23(2), 810–822.

Xue Long. Study on Deformation Behavior and Constitutive Model of Granular Materials under True Three-Dimensional Rotation of Principal Stress [D]. Tsinghua University, 2019.

Qian J , Du Z , Lu X ,et al. Effects of principal stress rotation on stress-strain behaviors of saturated clay under traffic-load-induced stress path[J].Soils and foundations, 2019, 59(1):41-55.

Zhe, M., Dong, T., Zhang, Y. F., et al. (2024). The Influence of Principal Stress Direction on the Deformation and Failure of Red Clay. Chinese Journal of Underground Space and Engineering, 20(1), 99-106.

Liu, C., Dong, T., Kong, L., et al. (2024). Experimental study on strength and shear band characteristics of sand under biaxial rotation of principal stresses. Chinese Journal of Rock Mechanics and Engineering, 43(7), 1809-1820.

Jamil, F., Zeng, C. N., Ma, Y., et al. (2025). Effect of initial consolidation inclination on strain development in saturated silty soil. Rock and Soil Mechanics, 46(2), 527-538.

Li Liang. Width of Stopping Mining Pillar and Surrounding Rock Control of Gateway Affected by Mining in Fully-Mechanized Top-Coal Caving Mining of Close-Distance Thick Coal Seams [D]. China University of Mining and Technology (Beijing), 2023.

Liu, J.-S., Zhu, K.-X., Zuo, J.-P., et al. (2024). The shear stress strain characteristics of weakly cemented soft rock under roadway excavation stress path and its non-coaxial characteristics. Chinese Journal of Rock Mechanics and Engineering, 43(4), 934-950.

Zuo J, Ma Z, Xu C, et al. Mechanism of principal stress rotation and deformation failure behavior induced by excavation in roadways[J]. Journal of Rock Mechanics and Geotechnical Engineering, 2024, 16(11): 4605-4624.

Li Jingjing. Research on interaction between surrounding rock and support by TBM techniques [D]. China University of Mining and Technology (Beijing), 2015.

Zuo J , Ma Z .Asymmetric deformation and failure behavior of roadway subjected to different principal stress based on biaxial tests[J].Tunnelling and Underground Space Technology incorporating Trenchless Technology Research, 2025, 155.

Feng Q , Zhang W , Liu W ,et al.Analytical solution of stress and displacement of surrounding rock in shallow buried tunnels with different hole-type under surface load[J].Tunnelling and Underground Space Technology incorporating Trenchless Technology Research, 2025, 159.

Dong Yucang. Study on mechanical characteristic of typical soft rock and design method of tunnel under high geo-stress condition [D]. Southwest Jiaotong University, 2020.

Yang, G. T. Introduction to Elastoplastic Mechanics[M]. Tsinghua University Press, 2013.

Brady B H G , Bray J W .The boundary element method for determining stresses and displacements around long openings in a

triaxial stress field[J].International Journal of Rock Mechanics and Mining Science & Geomechanics Abstracts, 1978, 15(1):21-28.

Zheng, Y. T. Theoretical Foundations of Elasto-Plasto-Viscosity in Rock Mechanics[M]. Coal Industry Press, 1988.

Wang, H. Y., Zhang, Q., Wu, P. N., et al.Closed-form solution for a circular roadway in elasto-plastic rock masses based on the generalized Hoek-Brown yield criterion[J]. Journal of Mining and Safety Engineering, 2025, 42(04): 789-797.

Gercek T U .Effect of Poisson's ratio on the normalized radial displacements occurring around the face of a circular tunnel[J].Tunnelling and Underground Space Technology, 2003.

Wang J , Li E , Chen L ,et al.Measurement and analysis of the internal displacement and spatial effect due to tunnel excavation in hard rock[J].Tunnelling and Underground Space Technology, 2019, 84(FEB.):151-165.

Fang Q , Wang G , Yu F ,et al.Analytical algorithm for longitudinal deformation profile of a deep tunnel[J].Journal of Rock Mechanics and Geotechnical Engineering, 2021, 13(5).

Guo J , Huang W , Feng G ,et al.Stability analysis of longwall top-coal caving face in extra-thick coal seams based on an innovative numerical hydraulic support model[J].International Journal of Mining Science and Technology, 2024, 34(4):491-505.

Zhang Q , Zhang X P , Wang H J ,et al.Numerical Study of the Effect of Grout Material Properties on Ground Deformation during Shallow TBM Tunneling[J].KSCE journal of civil engineering, 2022.

Chen T , Mitri H S .Strategies for surface crown pillar design using numerical modelling – A case study[J].International Journal of Rock Mechanics and Mining Sciences, 2021, 138(12):104599.